AIAA 99-3781

Computation of Turbulent Wake Flows in Variable Pressure Gradient

N. Duquesne
Royal Institute of Technology, KTH
Stockholm, Sweden

J.R. Carlson, C. L. Rumsey, and T. B. Gatski
NASA Langley Research Center
Hampton, Virginia, USA

30th AIAA Fluid Dynamics Conference
June 28 - July 1, 1999/Norfolk, VA

COMPUTATION OF TURBULENT WAKE FLOWS IN VARIABLE PRESSURE GRADIENT

N. Duquesne*, J. R. Carlson†, C. L. Rumsey‡, and T. B. Gatski§

Abstract

Transport aircraft performance is strongly influenced by the effectiveness of high-lift systems. Developing wakes generated by the airfoil elements are subjected to strong pressure gradients and can thicken very rapidly, limiting maximum lift. This paper focuses on the effects of various pressure gradients on developing symmetric wakes and on the ability of a linear eddy viscosity model and a nonlinear explicit algebraic stress model to accurately predict their downstream evolution. In order to reduce the uncertainties arising from numerical issues when assessing the performance of turbulence models, three different numerical codes with the same turbulence models are used. Results are compared to available experimental data to assess the accuracy of the computational results.

1 Introduction

Within the airframe industry, the optimal design of efficient high-lift devices for take-off and landing conditions is an important issue and one of the most challenging problems. For the current generation of commercial aircraft, such high-lift systems require a simplicity of design but a high level of efficiency. Achieving this goal demands improved Computational Fluid Dynamics (CFD) design tools that can realistically model the high-lift system flow field for full scale free flight Reynolds numbers. Difficulties are inherent to both the geometric complexity of multi-element airfoils as well as limitations in flow physics modeling. The flow field surrounding a multi-element airfoil is dominated by very complex viscous flow phenomena such as boundary layer transition, laminar separation bubbles, confluent turbulent boundary layers, multiple viscous wake interactions, and possible shock/boundary layer interactions. For this reason, the demands are high on the numerical methods used in this type of calculation, and several crucial aspects must be treated in an adequate way. One of these aspects is turbulence modeling.

In recent studies,[1,2] analyses of high-lift multi-element airfoil configurations were performed to assess the predictive capability of different types of turbulence models. The studies revealed three areas where turbulence model predictions were possibly deficient and which affected the overall prediction of the flow field. These areas were the inability to predict transition location, the inability to predict the slat wake, and the inability to properly account for streamwise curvature effects in the main element/flap region. Using the multi-element airfoil configuration, it is difficult to separate these effects. In this study, the dynamics of a developing symmetric wake generated by a splitter plate is studied by focusing on the ability of two turbulence models to predict its downstream evolution in different types of pressure fields. While the majority of previous studies have focused on fully developed wakes far downstream of their origin,[3] the emphasis here is the "near" wake region downstream of the slat.

Experimental studies which have isolated pressure gradient effects on a developing wake are rather scarce.[4] In this paper, numerical results are compared to the experimental results obtained at the University of Notre Dame (USA).[5] This experiment, which isolated the effect of pressure gradient on the development of a 2-D wake, has been specially designed to provide high quality data for use by the CFD community to validate turbulence models for wake flows.

In addition to having a well-documented experimental study, it is of equal importance to be able to evaluate the turbulence models within a numerical code whose numerical characteristics are well known.

*Research Associate, Royal Institute of Technology, KTH, Department of Aeronautics, SE-10044 Stockholm, Sweden, Member AIAA.

†Senior Research Scientist, Subsonic Aerodynamics Branch, NASA LaRC, Hampton VA, Senior Member AIAA.

‡Senior Research Scientist, Aerodynamic and Acoustics Methods Branch, NASA LaRC, Hampton VA, Senior Member AIAA.

§Senior Research Scientist, Aerodynamic and Acoustics Methods Branch, NASA LaRC, Hampton VA.

Even then it is optimal, although difficult, to perform the validation studies using different numerical codes in order to quantify any numerical biases. The challenge in this regard is then to be sure that each turbulence model is similarly implemented into the different codes. This level of effort is time consuming, but becoming more essential in the current technical environment where an increasing number of ill-posed validation studies are being undertaken.

The purpose of this paper is to describe a validation study in which three different numerical codes CFL3D,[6] NSMB,[7] and PAB3D[8,9] are used to validate two different types of turbulence models on a near wake flow in zero, adverse, and favorable pressure gradients. The two different types of turbulence models include a linear isotropic eddy viscosity model[10] and an explicit algebraic stress model.[11]

The next section describes briefly the experimental study performed at the University of Notre Dame. Then, the turbulence models are presented and the main differences between the three codes are highlighted. For each code, the linear isotropic eddy viscosity model and the explicit algebraic stress model are first validated against experimental data obtained in a simple channel. The last part of the paper presents the results obtained by the three codes using these two types of turbulence models for wake flows subjected to different types of pressure gradients.

2 Experimental Data

The data used in this study is the result of an experimental research program on wake development in different pressure gradients. This work is a collaborative effort between the Hessert Center for Aerospace Research at the University of Notre Dame (USA) and the NASA Langley Research Center (USA). With this carefully controlled experiment, it has been possible to isolate the effect of pressure gradient on the development of a 2-D wake in conditions similar to that experienced by the slat wake of a multi-element airfoil. One of the unique features of this experiment was the elimination of unnecessary complicating factors such as wake/boundary layer interaction and cove separation, which are present on real airfoil and wing configurations and can make meaningful CFD assessments an extremely difficult task.

The two-dimensional wake experiments were performed in a low-speed wind tunnel facility. The Reynolds number was approximately 2.4×10^6 based on the length of the wake-generating body. For comparison, it may be noted that a Boeing 737-100 operating at a Reynolds number (based on mean average chord) of 15.7×10^6 during landing approach has a Reynolds number of about 1.8×10^6 based on slat chord.[5] The wake-generating body is a two-dimensional splitter plate with round nose and tapered trailing edge. The boundary layer on the flat plate is tripped by distributed roughness over the nose. The splitter plate (1.2192 m long) is used to generate the wake. The wind tunnel section with adjustable tunnel walls located immediately downstream of the wake-generating body is used to produce the desired pressure gradient environment for wake development. By using the adjustable walls, the initial degree of asymmetry can also be controlled. To date, the experimental study has been limited to the study of the structure and development of symmetric wakes.

For different combinations of imposed pressure gradients, experimental mean velocity and turbulence data were compiled using hot wire and two-component Laser Doppler Velocimetry measurements. Experimental results have verified the two-dimensionality of the flow field. They have also shown the effects of favorable and adverse pressure gradients on wake thickening and velocity defect decay. Note that a Reynolds stress bias error discovered in the $u'v'$ measurements in Liu et al[5] has been corrected. See Liu[12] for more details.

3 Numerical Approach

3.1 Turbulence models

Two-equation turbulence models represent the simplest level of closure that contains transport equations for both the characteristic velocity and length scale. However, it is well known that models based on the Boussinesq eddy viscosity concept lack the universality required as they provide a somewhat restrictive representation of the physical processes governing the Reynolds stress tensor. Typically, they do not adequately account for the stress anisotropies induced by the flow. The Differential Stress Model (DSM) devised by reference to the exact but unclosed equation for the Reynolds stress tensor can properly account for the advective and diffusive transport of the Reynolds stress tensor but is much more complicated and too expensive for many practical engineering applications. As an alternative, explicit algebraic stress models have been developed. They provide a close coupling with the DSM in that they are directly derivable from the stress transport equations subject to constraints on the advection and diffusion terms. Thus, these models retain the characteristics of the full DSM introduced through the pressure-strain correlation model but also bring some economy to the compu-

tation. In this study, two turbulence models have been selected: a linear, isotropic eddy-viscosity K-ε model (EVM),[10] and an explicit algebraic stress model (EASM).[11]

3.2 Linear Eddy Viscosity K-ε model

The linear eddy viscosity model used in this study is based on the $K-\varepsilon$ model of Speziale and Abid.[10] The modeled transport equations are the following:

$$\frac{DK}{Dt} = \mathcal{P} - \varepsilon + \frac{\partial}{\partial x_i}\left[\left(\nu + \frac{\nu_t}{\sigma_K}\right)\frac{\partial K}{\partial x_i}\right] \qquad (1)$$

$$\frac{D\varepsilon}{Dt} = C_{\varepsilon 1}\frac{\varepsilon}{K}\mathcal{P} \; - \; C_{\varepsilon 2} f_\varepsilon \frac{\varepsilon^2}{K} + \frac{\partial}{\partial x_i}\left[\left(\nu + \frac{\nu_t}{\sigma_\varepsilon}\right)\frac{\partial \varepsilon}{\partial x_i}\right] \qquad (2)$$

with

$$C_{\varepsilon_1} = 1.44, \quad C_{\varepsilon_2} = 1.83$$

$$\sigma_K = 1.0, \quad \sigma_\varepsilon = \frac{\kappa^2}{(C_{\varepsilon_2} - C_{\varepsilon_1})\sqrt{(C_\mu)}}, \quad \kappa = 0.41,$$

where $D/Dt = \partial/\partial t + u_i \partial/\partial x_i$, $\mathcal{P}$ is the production of turbulent kinetic energy ($= -\tau_{ij}\partial u_i/\partial x_j$), τ_{ij} is the Reynolds stress tensor ($= -\nu_t(\partial u_i/\partial x_j + \partial u_j/\partial x_i)$, $K(= \frac{1}{2}\tau_{nn})$ is the turbulent kinetic energy, ε is the turbulent dissipation rate, and ν_t is defined as $\nu_t = C_\mu K^2/\varepsilon$, where $C_\mu = 0.09$.

The role of the function f_ε is to remove the singularity in the destruction of the dissipation term; its expression is given by:

$$f_\varepsilon = 1 - \exp(-Re_K/12), \qquad (3)$$

with $Re_K = \sqrt{K}d/\nu$ the Reynolds number based on the distance to the nearest wall.

3.3 Explicit Algebraic Stress Model

The development of the explicit algebraic stress model (EASM) used in this study is outlined in detail in Rumsey et al.[11] It is based on the formulation developed by Jongen and Gatski[13] from the earlier work of Pope[14] and Gatski and Speziale.[15] The reader is referred to these earlier studies for additional background. The resulting EASM for the anisotropy tensor

$$b_{ij} = \frac{\tau_{ij}}{2K} - \frac{1}{3}\delta_{ij} \qquad (4)$$

in two-dimensional flows is given by

$$\mathbf{b} = \alpha_1\mathbf{S} + \alpha_2(\mathbf{SW} - \mathbf{WS}) + \alpha_3\left(\mathbf{S}^2 - \frac{1}{3}\{\mathbf{S}^2\}\mathbf{I}\right), \qquad (5)$$

where $\mathbf{S}$ $(= S_{ij})$ and $\mathbf{W}$ $(= W_{ij})$ are the strain rate and rotation rate tensors, respectively,

$$S_{ij} = \frac{1}{2}\left(\frac{\partial u_i}{\partial x_j} + \frac{\partial u_j}{\partial x_i}\right), \quad W_{ij} = \frac{1}{2}\left(\frac{\partial u_i}{\partial x_j} - \frac{\partial u_j}{\partial x_i}\right),$$

and the α_i are scalar coefficient functions of the invariants $\eta^2(= \{\mathbf{S}^2\})$ and $\mathcal{R}^2(= -\{\mathbf{W}^2\}/\{\mathbf{S}^2\})$. The coefficients α_1, α_2, and α_3 are given by[11]

$$\gamma_0^2\alpha_1^3 - \frac{\gamma_0\gamma_1}{\eta^2\tau}\alpha_1^2 + \frac{1}{4\eta^4\tau^2}\left[\gamma_1^2 - 2\tau^2\gamma_0\{\mathbf{RS}\} - 2\eta^2\tau^2\left(\frac{a_3^2}{3} - \mathcal{R}^2 a_2^2\right)\right]\alpha_1 + \frac{1}{4\eta^6\tau}\left[\gamma_1\{\mathbf{RS}\} + 2\tau\left(a_2\{\mathbf{RWS}\} - a_3\{\mathbf{RS}^2\}\right)\right] = 0, \qquad (6)$$

$$\alpha_2 \; = \; a_4\left[a_2\alpha_1 + \frac{\{\mathbf{RWS}\}}{\eta^4\mathcal{R}^2}\right], \qquad (7)$$

$$\alpha_3 \; = \; -a_4\left[2a_3\alpha_1 + \frac{6\{\mathbf{RS}^2\}}{\eta^4}\right], \qquad (8)$$

where $\alpha_0 = \left(1 - \frac{2}{3}a_3^2a_4^2\eta^2 + 2a_2^2a_4^2\eta^2\mathcal{R}^2\right)$ and $\tau = K/\varepsilon$. When $\mathbf{R} = a_1\mathbf{S}$, then $\{\mathbf{RWS}\} = \{\mathbf{RS}^2\} = 0$ and $\{\mathbf{RS}\} = a_1\eta^2$. The coefficients a_i are directly related to the pressure-strain correlation model used in closing the stress transport equation. This study uses the SSG pressure-strain model,[16] which yields

$$a_1 = \frac{1}{2}\left(\frac{4}{3} - C_2\right), \quad a_2 = \frac{1}{2}(2 - C_4), \quad a_3 = \frac{1}{2}(2 - C_3), \quad a_4 = g\tau, \qquad (9)$$

and

$$g \; = \; \left[\left(\frac{C_1^1}{2} + 1\right)\frac{\mathcal{P}}{\varepsilon} + \frac{C_1^0}{2} - 1\right]^{-1} \qquad (10)$$

$$= \; \left[\gamma_1 + \gamma_0\frac{\mathcal{P}}{\varepsilon}\right]^{-1} = \left[\gamma_1 - 2\gamma_0\alpha_1\eta^2\tau\right]^{-1} \qquad (11)$$

$$C_1^0 = 3.4(\gamma_1 = 0.7), \quad C_1^1 = 1.8(\gamma_0 = 1.9),$$
$$C_2 = 0.36, \quad C_3 = 1.25, \quad C_4 = 0.4.$$

The explicit tensor representation given in Eq. (5) is coupled with the K-ε two-equation model described in Eqs. (1)–(3). Only the coefficients C_μ and f_ε require slightly different values and are now given by

$$C_\mu = 0.096, \qquad f_\varepsilon = 1 - \exp\left(-\frac{Re_K}{10.8}\right). \qquad (12)$$

In the development of the algebraic stress model, two assumptions are made in the formulation of the implicit algebraic equation for the stress anisotropy. The first is an equilibrium assumption on the Reynolds stress anisotropy

$$\frac{Db_{ij}}{Dt} = \frac{D\tau_{ij}}{Dt} - \frac{\tau_{ij}}{K}\frac{DK}{Dt} = 0, \tag{13}$$

and the second is an assumption on the anisotropic behavior of the turbulent transport and viscous diffusion term $\mathcal{D}_{ij}$, that is

$$\mathcal{D}_{ij} - \frac{\tau_{ij}}{2K}\mathcal{D}_{nn} = 0. \tag{14}$$

Equation (14) assumes that the anisotropy in $\mathcal{D}_{ij}$ is directly related to the anisotropy in the Reynolds stresses themselves. However, Gatski and Rumsey[17] has shown that near the center region of wake flows Eq. (14) leads to unphysically large levels of turbulent eddy viscosity. A different constraint on $\mathcal{D}_{ij}$ can be found by rewriting Eq. (14) in terms of the anisotropy tensor b_{ij}. This leads to the modified constraint

$$\mathcal{D}_{ij} - \frac{1}{3}\mathcal{D}_{nn}\delta_{ij} = 0, \tag{15}$$

which simply states that the deviatoric part of the tensor $\mathcal{D}_{ij}$ is zero. The contribution from $b_{ij}\mathcal{D}_{nn}$ now appears as a modification to the a_4 coefficient in the form

$$\frac{1}{a_4^*} = \frac{1}{a_4} + \frac{1}{2K}\mathcal{D}_{nn}, \tag{16}$$

or

$$a_4^* = \left[\left(\gamma_1 + \frac{1}{\varepsilon}\frac{DK}{Dt} + 1\right) - 2\left(\gamma_0 - 1\right)\alpha_1\eta^2\tau\right]^{-1}\tau. \tag{17}$$

As is well known, the algebraic stress formulation should yield the same results as a full second-moment closure in the case of homogeneous shear. Thus a modification to the algebraic stress model as described here needs to maintain this relationship. This requirement can be fulfilled by invoking an equilibrium assumption on the turbulent time scale, that is

$$\frac{D\tau}{Dt} = \frac{1}{\varepsilon}\frac{DK}{Dt} - \frac{K}{\varepsilon^2}\frac{D\varepsilon}{Dt} = 0. \tag{18}$$

For the case of homogeneous shear, this yields the relationship

$$\frac{1}{\varepsilon}\frac{DK}{Dt} = \frac{K}{\varepsilon^2}\frac{D\varepsilon}{Dt} = C_{\varepsilon 1}\frac{\mathcal{P}}{\varepsilon} - C_{\varepsilon 2}, \tag{19}$$

which can be substituted into Eq. (17) along with the equilibrium condition on $\mathcal{P}/\varepsilon$,

$$\frac{\mathcal{P}}{\varepsilon} = \frac{C_{\varepsilon 2} - 1}{C_{\varepsilon 1} - 1} \tag{20}$$

to give

$$a_4^* = \left[\gamma_1^* - 2\gamma_0^*\alpha_1\eta^2\tau\right]^{-1}\tau, \tag{21}$$

where

$$\gamma_0^* = \gamma_0 - 1, \tag{22}$$

$$\gamma_1^* = \gamma_1 + 1 + \left(\frac{C_{\varepsilon 2} - C_{\varepsilon 1}}{C_{\varepsilon 1} - 1}\right). \tag{23}$$

The values for $C_{\varepsilon 1}$ and $C_{\varepsilon 2}$ are the same as those used in the linear EVM, that is, 1.44 and 1.83, respectively. This modification meets the requirement that the homogeneous shear results are unaltered, and only slightly affects the results for the log-layer where the value of C_μ is changed from 0.096 (see Eq. (12)) to 0.0885. The only other alterations to the algebraic stress formulation are that now a_4^*, γ_0^*, and γ_1^* are used instead of the coefficients a_4, γ_0, and γ_1.

3.4 Numerical Algorithms

In order to provide a controlled assessment of the performance of the turbulence models, they have been implemented into three different numerical codes CFL3D,[6] NSMB,[7] and PAB3D.[8,9] With this multiple-code implementation, the effect of the purely numerical influences on the solution results can be quantified. Many organized efforts at validating the performance of turbulence models suffer from the lack of precise coordination of detailed turbulence model implementation. In the validation study presented here, this deficiency is rectified and a more accurate assessment of the turbulence models can be made. The three codes solve the three-dimensional Reynolds-averaged compressible Navier-Stokes equations. The distinctive features of each code are briefly described in this section.

CFL3D

CFL3D is a computational method for structured grids developed at NASA Langley Research Center. The code uses an upwind finite volume formulation. It neglects viscous cross-derivative terms, which results in the thin-layer Navier-Stokes equations in specified coordinate directions. Third-order upwind-biased spatial differencing on the convective and pressure terms, and second-order differencing on the viscous terms are used; it is globally second-order spatially accurate. The CFL3D code can solve flow over multiple-zone grids that are connected in

a one-to-one, patched, or overset manner, and can employ grid sequencing, multi-grid, and local time stepping when accelerating convergence to steady state. Upwind-biased spatial differencing is used for the inviscid terms, and flux limiting is used to obtain smooth solutions in the vicinity of shock waves, when present. No limiter was employed for this study. Viscous terms are centrally differenced. The flux difference-splitting (FDS) method of Roe is employed to obtain fluxes at the cell faces. The CFL3D code is advanced in time with an implicit three-factor approximate factorization method. The implicit derivatives are written as spatially first-order accurate, which results in block-tridiagonal inversions for each sweep. However, for solutions that utilize FDS the block-tridiagonal inversions are further simplified with a diagonal algorithm. Turbulence equations are solved uncoupled from the mean equations.

NSMB

The NSMB (Navier-Stokes Multi-Block) code is a finite volume code for structured grids developed by two universities, EPFL (Switzerland) and KTH (Sweden), a research institute CERFACS (France), and two companies, Aérospatiale (France) and SAAB (Sweden). A cell-centered finite volume method is used, and the viscous cross-derivative terms are included in the formulation. The equations are discretized in space using either a central difference scheme yielding second order accuracy in space for a smooth grid with artificial dissipation (standard Jameson dissipation, Martinelli dissipation or matrix dissipation), or an upwind scheme (Roe and AUSM using different limiters). In this study, the central scheme with the standard Jameson dissipation has been used. The time integration can be achieved through the use of an explicit Runge-Kutta time stepping. For steady-state problems, an implicit time integration scheme is available in the form of the LU-SGS scheme of Yoon and Jameson[18] which is based on a Lower-Upper factorization and a symmetric Gauss Seidel relaxation. The turbulence equations are solved coupled to the mean equations.

PAB3D

PAB3D[8,9] is a code developed by Analytical Services and Materials, Inc. for structured grids using an upwind finite volume formulation. It can either solve thin-layer Navier-Stokes or any two grid-index directions with fully coupled viscous terms. In this study, the two directions were uncoupled as in CFL3D. The Roe FDS scheme is used to evaluate the explicit part of the governing equations and the van Leer scheme is used to construct the implicit operator. The FDS solutions with this method were not further simplified with a diagonal algorithm which should only impact solution time and not solution accuracy. The diffusion terms are centrally differenced, and the inviscid flux terms are upwind differenced. Similar to CFL3D, several different flux limiters can be applied. Current solutions used the min-mod flux limiter. Both the mean and turbulent flow equations used a third-order-accurate scheme for the convective terms and second-order accurate for the viscous diffusion terms. The turbulent flow equations are solved uncoupled from the mean flow equations.

4 Results and Discussion

4.1 Turbulence model validation

As a first step in the process of turbulence model calibration and validation, all three codes CFL3D, PAB3D, and NSMB used the two-equation turbulence model (EVM) and explicit algebraic stress model (EASM) described in the previous section to compute the channel flow of Laufer.[19] The same grid was used in all three codes. The grid models half the channel and consists of 89×73 gridpoints. The cells are clustered close to the wall in the y direction and equally spaced in the x direction. The mean value of y^+ at the first gridpoint off the wall is below 1.

The free-stream Mach number is set to 0.2, and the Reynolds number based on the freestream velocity and half of the channel width is 61600. The total pressure and total temperature are prescribed at the inlet. A back static pressure is imposed at the outlet. As shown in Figs. 1 and 2, both mean flow and turbulence quantities are in a very close agreement for the three CFD codes when either the EVM or EASM are employed. In general, both turbulence models yield results in good agreement with experiment. As expected, the eddy viscosity model cannot predict a difference between the normal Reynolds stress components (Fig. 1d), whereas the normal stress components predicted by the EASM (Fig. 2d) show the correct trends.

4.2 Wake Flow

4.2.1 Numerical implementation

The computational domain for the wake flow test case (zero pressure gradient) is depicted in Fig. 3. The domains for the adverse and favorable conditions have different tunnel wall shapes downstream of the splitter plate. The overall geometry is identical to the experimental one, except that an elliptic nose is used for the splitter plate instead of a circular nose. Initial computations with a circular

nose showed a large laminar separation bubble that was quite difficult to compute and some unsteadiness was noticed. Because the experimental tests included roughness over the nose to trip the boundary layer on the plate, the laminar bubble probably did not exist in the experiments, although the experimental data were insufficient in this region to verify this. The use of an elliptic nose in the computational study eliminates the laminar bubble.

Consistent with experimental conditions, no-slip and adiabatic wall conditions are assumed at solid walls. At the inflow boundary, the total pressure and total temperature are specified, and at the outflow boundary, the back static pressure is specified. As in the experimental study, zero, adverse and favorable pressure gradients are attained in the numerical study by using a different geometry for the tunnel wall shape. It was necessary to test different back pressures for each of the test cases to recover the experimental velocity at the end of the splitter plate; these tests have been carried out essentially with CFL3D. Then, for each test case, the ratio of the static pressure at the outflow $P_{outflow}$ over the total pressure at the inflow $P_{t_{inflow}}$ has been fixed at the same value in all three codes. Because PAB3D is not a non-dimensional code and because computations for these test cases with NSMB used physical values as well, the pressure and temperature ratios used in CFL3D were converted to equivalent metric quantities assuming a freestream total pressure of 101.325 KPa and total temperature of 300 K.

Because the wakes are assumed symmetric,[5] computations are only performed on the upper half of the computational domain and a symmetric boundary condition is imposed in the center of the tunnel. This minimizes grid points and allows for a greater concentration of the points in regions of interest. An early study with CFL3D confirmed that identical results were obtained using a half domain or full one.

Computational grids, comprised of 5 blocks, used a high concentration of points near the walls, plate surface and in the wake. All grids were generated with an average distance from the wall to the first gridpoint of approximately $y^+ = 1.1$. The total number of points in the finest mesh is 63549.

Grid dependence tests have been performed using CFL3D on three different grids (each successively coarser grid made up of every other point from the finer levels). Of the cases tested, the favorable pressure gradient test case showed the greatest sensitivity to grid size. The velocity and turbulent shear stress sensitivities for this case using the EVM can be seen in Figs. 4 and 5. The trends suggest that further mesh refinement may be useful, but should not yield significantly different results from the fine grid. Although not shown, results for the zero pressure gradient test case showed almost no sensitivity in the velocity profiles. Sensitivities using EASM were similar to EVM.

Because the turbulence models are not able to accurately predict transition location, the point of transition was different for each model as well as for each code. In all the tests, the codes were run "fully turbulent": transition location was not fixed but the respective models and codes were allowed to transition freely. Resulting transition locations for both EVM and EASM are summarized in Tables 1 and 2, respectively, for the adverse pressure gradient (APG), zero pressure gradient (ZPG), and favorable pressure gradient (FPG) cases. In general, PAB3D tends to transition somewhat further downstream than CFL3D; however, as will be shown later, these differences do not lead to significant differences in the computed solutions at the end of the plate. With the exception of FPG using EVM, NSMB's transition locations are consistently further downstream than the other codes.

	CFL3D	NSMB	PAB3D
APG	0.053	0.370	0.368
ZPG	0.064	0.355	0.206
FPG	0.150	0.057	0.226

Table 1. Transition x-location in meters along the splitter plate using EVM.

	CFL3D	NSMB	PAB3D
APG	0.056	0.370	0.333
ZPG	0.099	0.345	0.213
FPG	0.191	0.310	0.180

Table 2. Transition x-location in meters along the splitter plate using EASM.

4.2.2 Zero Pressure Gradient

The zero pressure gradient wake test case is computed to serve both as a baseline for comparison with variable pressure gradient wake development and as a comparative check on the predictions of the three codes using the same turbulence models.

The symmetric turbulent wake generated by a splitter plate is typically divided into three regions. The first region begins at the end of the plate and may extend to approximately 25 momentum thicknesses, which corresponds in this study to the lo-

cation $x = 1.3\ m$. The second, or intermediate, region modifies the logarithmic region of the plate boundary layer. The third, or far wake, region begins about 350 momentum thicknesses downstream of the trailing edge where the mixing is complete.[20] This last region is located at $x = 2.3\ m$ in this study.

As an initial comparison of code and model behavior, predictions from the three codes were compared to experimental mean velocity and shear stress data at $x = 1.2167\ m$, near the end of the splitter plate. The velocity profiles (see Fig. 6) predicted by CFL3D and PAB3D show good agreement with experimental data for both the EVM and EASM, whereas NSMB leads to a fuller profile and a smaller boundary layer thickness in both cases. The shear stress profiles at the same location (see Fig. 7) show greater variation in the case of EASM, and the agreement with experiment is not as good as the mean velocities for either turbulence model.

Because great pains were taken to ensure the same implementation of the turbulence models in all three codes (recall the channel flow validation study), the variations in the results for this more complex case are somewhat disappointing. One possible cause for the variations may be the different numerics in the three codes: NSMB uses a central scheme with the standard Jameson dissipation and CFL3D and PAB3D use an upwind scheme. However, while a grid study with NSMB (not shown) indicates a somewhat greater sensitivity to grid than CFL3D, its trend shows decreasing boundary layer thickness with increasing grid density. This trend does not account for the differences seen in Fig. 6.

Another possible cause for the different results is the fact that the three codes transition in different locations. In Tables 1 and 2, the transition locations for ZPG are successively further downstream (by between 0.1 and 0.15 m) for the three codes. This difference does not seem to affect the results between CFL3D and PAB3D, but it is possible that NSMB's transition location is far enough downstream to cause a noticeable difference in results near the trailing edge.

The computed mean velocity profiles in the wake are compared with the experimental results in Figs. 8 and 9. In the near wake (Figs. 8a and 9a), the agreement between numerical and experimental velocity profiles is still very good overall; whereas, further downstream (Figs. 8b,c and 9b,c) the velocity in the wake is slightly overpredicted by all codes. The initial fuller profile displayed by the NSMB code persists, but the qualitative trend is the same as both the CFL3D and PAB3D codes.

Figures 10 and 11 show the comparison between the computed shear stress and experimental data. In the near wake region (Figs. 10a and 11a), the computed results are in good overall agreement with the experimental data. Further downstream in the wake, the computed shear stresses (Figs. 10b,c and 11b,c) decrease too fast compared to the experimental data. It is interesting to note that the qualitative trends are not dependent on the choice of turbulence model. Thus, the added physics associated with the EASM, such as better accounting for stress anisotropy and closer sensitivity to gradients of the mean velocity, do not play a significant role in the prediction of the developing wake flows.

It should be noted that while transition location and numerical differences (such as central differencing vs. upwind differencing) are likely to be the cause of most of the differences observed between the three codes, various implementation details in the codes are also very different and may be factors. Some examples include the order of accuracy of the turbulent advective terms, type of flux limiter, method for including the nonlinear turbulent stress terms, and nondimensionalization relative to the boundary conditions. These types of differences were too numerous to explore for this study.

4.2.3 Adverse Pressure Gradient

The experimental results have shown that the influence of the pressure gradient on wake development and structure is very significant.[5] When an adverse pressure gradient is imposed, the wake width is increased and the Reynolds shear stress is amplified (relative to ZPG).

The nominal pressure gradient in the wake for this case is $dC_p/dx = 0.3386/m$. Numerical results for the mean velocity obtained with the three different codes are in good agreement with experimental results for both the EVM (Fig. 12) and the EASM (Fig. 13) models. The computed turbulent shear stresses are shown in Figs. 14 and 15. The computed shear stresses over-predict the local maximum experimental data initially and then further downstream under-predict the experimental results. In comparison with the corresponding zero pressure gradient case (Figs. 8 – 11), the numerical predictions for the adverse pressure gradient case are better and the results are more consistent between the different codes.

4.2.4 Favorable Pressure Gradient

When the wake develops in a favorable pressure gradient, the wake width is reduced and the Reynolds stress is decreased (relative to ZPG). Because in all cases the numerical results for both the

EVM and the EASM are very similar, for brevity only the EASM results are shown here.

The nominal pressure gradient in the wake for this case is $dC_p/dx = -0.5984/m$. In Fig. 16 the development of the mean velocity profiles is shown. As in the adverse pressure gradient case, all three codes underpredict the wake thickness at $x = 1.3462\ m$ (Fig. 16a). The wake deficit is also slightly off. At the intermediate station (Fig. 16b) the computed results continue to overpredict the mean velocity, while at the last station (Fig. 16c) the computed results are becoming more in line with the experiment. The computed turbulent shear stress profiles are shown in Fig. 17. The trends here are similar to the zero and adverse pressure gradient cases.

5 Conclusions

A purpose of this paper was to describe a study in which three different numerical codes, CFL3D, NSMB, and PAB3D, are used to validate two different types of turbulence models on a near wake flow in zero, adverse, and favorable pressure gradients. The two different types of turbulence models included a linear isotropic eddy viscosity model (EVM) and an explicit algebraic stress model (EASM).

In order to perform as credible a validation study as possible, the turbulence models were implemented as identically as possible in each code. Then, for validation of each code, the EVM and EASM results were compared to experimental data obtained in a simple channel. Results showed excellent agreement among the three codes.

The three codes were then applied to the study of symmetric turbulent wakes. Comparisons between the numerical results and the experimental data yielded the following conclusions:

- Mean velocity profiles for the three different pressure gradient conditions are, in general, in good agreement with the experimental profiles
- More significant discrepancies are observed for the turbulent quantities, although both the EVM and EASM are able to qualitatively reproduce the experimental results
- Although small differences exist, the EVM and EASM lead to very similar results

The differences between computed results from the three codes for the wake cases cannot be attributed to the turbulence models, which are identical in each code, but rather to the differences in transition location and numerical differences between the codes. Further study into the influence of the numerical scheme as well as the influence of the artificial dissipation, especially on the turbulent stress results, is needed. A method for guaranteeing transition in a consistent fashion between different codes (when running "fully turbulent") should be explored.

As discussed in the Introduction, the motivation for this study was to try to isolate the predictive capability of turbulence models on developing wake flows which have relevance to the wakes shed from airfoil elements, such as slats, in high-lift systems. Such wakes develop in strong pressure gradients, and are an integral part of the aerodynamics of the high-lift system. The present study has shown that the inclusion of the effects of turbulence anisotropy and/or improved sensitivity to the mean velocity gradient field are not central to the accurate description of near wake development. Even a simple two-equation eddy viscosity turbulence model can reproduce the near-wake development fairly well in the three pressure fields studied.

However, it should be noted that the pressure gradients experienced by a slat wake are typically variable (a short, very strong favorable gradient followed by an adverse gradient), and these gradients can be significantly stronger than those imposed in this wake study. A potentially useful future experimental study would attempt to duplicate the variable pressure field levels seen by a typical slat wake.

A final important conclusion from this study is that turbulence models can easily be (and often are) coded differently in different CFD codes. Small variations in the models (constants, damping functions, etc.) can completely alter computed results and muddy the conclusions. Ensuring identical turbulence model implementation is tedious; however, it is well worth the effort. Using multiple CFD codes for a turbulence model validation study accomplishes the following. First, it gives confidence that each turbulence model has been implemented correctly, and, as a result, it is easier to draw conclusions regarding the turbulence model itself. Second, when transition location is the same, differences between the codes' results may be solely attributed to differences in the codes' numerics; this is helpful for establishing limits on the numerical uncertainty for a given case.

Acknowledgments

The authors gratefully acknowledge X. Liu and F. Thomas of the University of Notre Dame (USA) for their thoroughness in extracting and preparing the data, as well as their responsiveness to questions and concerns that arose during the course of this study. Also, the use of computer time from NSC, the Na-

tional Supercomputer Centre, Linköping University is acknowledged by the first author.

References

1. **Rumsey, C.L., Gatski, T.B., Ying, S.X., and Bertelrud, A.**, "Prediction of High-Lift Flows using Turbulent Closure Models", *AIAA Journal*, Vol. 36, No. 5, 1998, pp. 765–774.

2. **Ying, S.X., Spaid, F.W., McGinley, C.B., and Rumsey, C.L.**, "Investigation of Confluent Boundary Layers in High-Lift Flows", *Journal of Aircraft*, Vol. 36, No. 3, 1999, pp. 550–562.

3. **Marasli, B., Champagne, F.H., and Wygnanski, I.**, "Effect of Travelling Waves on the Growth of a Plane Turbulent Wake", *J. Fluid Mech.*, Vol. 235, 1991, pp. 511–528.

4. **Hoffenberg, R., Sullivan, J.P., and Schneider, S.P.**, "Wake Measurements in a Strong Adverse Pressure Gradient", AIAA 95-1912, 13th AIAA Applied Aerodynamics Conference, San Diego CA, June 1995.

5. **Liu, X., Thomas, F.O., and Nelson, R.C.**, "An Experimental Investigation of Wake Development in Arbitrary Pressure Gradient", AIAA 99-0677, 37th Aerospace Sciences Meeting & Exhibit, Reno NV, January 1999.

6. **Krist, S.L., Biedron, R.T., and Rumsey, C.L.**, "CFL3D User's Manual (Version 5.0)", NASA TM-1998-208444, June 1998.

7. **Vos, J.B., Rizzi, A.W., Corjon, A., Chaput, E., and Soinne, E.**, "Recent Advances in Aerodynamics inside the NSMB (Navier-Stokes Multi Block) Consortium", AIAA 98-0225, 36th Aerospace Sciences Meeting & Exhibit, Reno NV, January 1998.

8. **Abdol-Hamid, K.S.**, "Implementation of Algebraic Stress Models in General 3D Navier Stokes Method (PAB3D)", NASA CR-4702, December 1995.

9. **Carlson, J.R.**, "Applications of Algebraic Reynolds Stress Turbulence Models Part 1: Incompressible Flat Plate", *Journal of Propulsion and Power*, Vol. 13, No. 5, 1997, pp. 610–619.

10. **Speziale, C.G. and Abid, R.**, "Near Wall Integration of Reynolds Stress Turbulence Closures with No Wall Damping", *AIAA Journal*, Vol. 33, No. 10, 1995, pp. 1974–1977.

11. **Rumsey, C.L., Gatski, T.B., and Morrison, J.H.**, "Turbulence Model Predictions of Extra-Strain Rate Effects in Strongly-Curved Flows", AIAA 99-0157, 37th Aerospace Sciences Meeting & Exhibit, Reno NV, January 1999.

12. **Liu, X.**, "A Bias Error Correction Method for LDV Reynolds Stress Measurements in the Symmetric Wake", University of Notre Dame Technical Memo No. 99-1, April 1999.

13. **Jongen, T. and Gatski, T.B.**, "General Explicit Algebraic Stress Relations and Best Approximation for Three-Dimensional Flows", *Int. J. Engr. Sci.*, Vol. 36, 1998, pp. 739–763.

14. **Pope, S.B.**, "A More General Effective Viscosity Hypothesis", *J. Fluid Mech.*, Vol. 72, 1975, pp. 331–340.

15. **Gatski, T.B. and Speziale, C.G.**, "On Explicit Algebraic Stress Models for Complex Turbulent Flows", *J. Fluid Mech.*, Vol. 254, 1993, pp. 59–78.

16. **Speziale, C.G., Sarkar, S., and Gatski, T.B.**, "Modeling the Pressure-Strain Correlation of Turbulence: an Invariant Dynamical Systems Approach", *J. Fluid Mech.*, Vol. 227, 1991, pp. 245–272.

17. **Gatski, T.B., and Rumsey, C.L.**, "Linear and Non-Linear Eddy Viscosity Models", *Closure Strategies for Turbulent and Transitional Flows*, (B. E. Launder and N. D. Sandham, eds.), Cambridge University Press, To Appear, 1999.

18. **Yoon, S. and Jameson, A.**, "A Multigrid LU-SOOR Scheme for Approximate Newton Iteration Applied to the Euler Equations", NASA-CR-179524, 1986.

19. **Laufer, J.**, "Investigation of Turbulent Flow in a Two-Dimensional Channel", NACA Report 1053, 1950.

20. **Ramaprian, B.R. and Patel, V.C.**, "The symmetric Turbulent Wake of a Flat Plate", *AIAA Journal*, Vol. 20, No. 9, 1978, pp. 80–89.

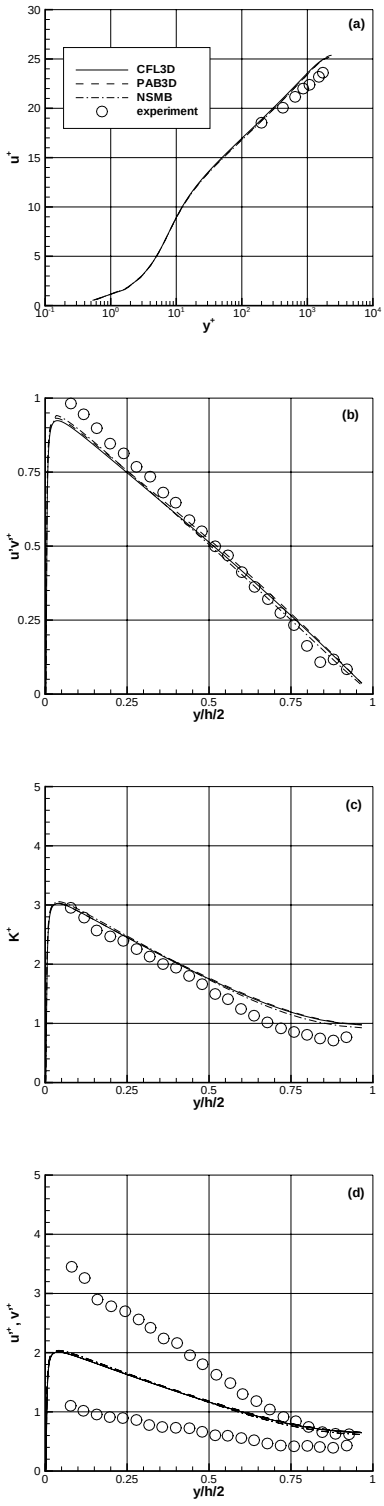

Figure 1. Fully developed turbulent channel flow[19] predictions with EVM: (a) Mean velocity, (b) Reynolds shear stress, (c) turbulent kinetic energy, (d) Reynolds normal stresses

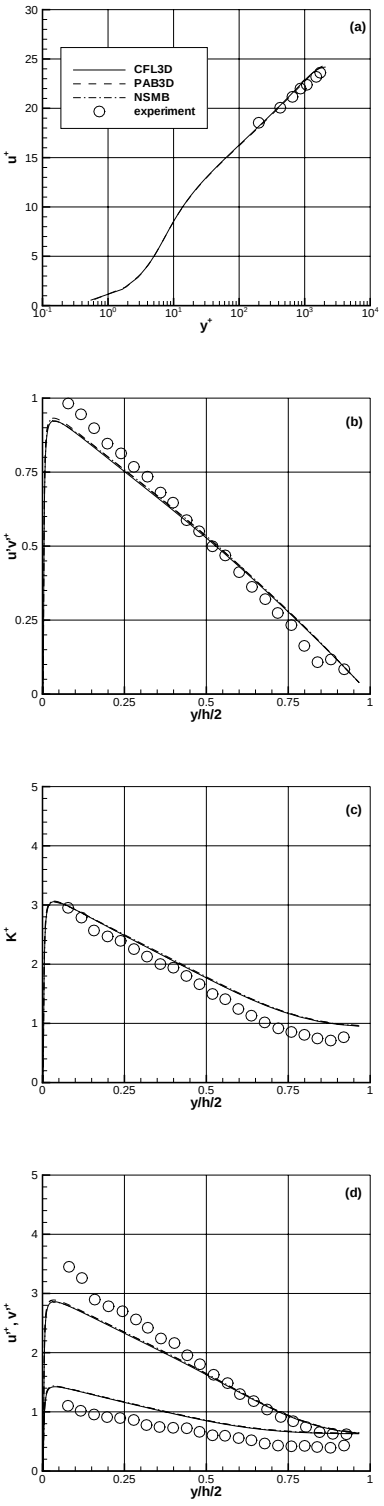

Figure 2. Fully developed turbulent channel flow[19] predictions with EASM: (a) Mean velocity, (b) Reynolds shear stress, (c) turbulent kinetic energy, (d) Reynolds normal stresses

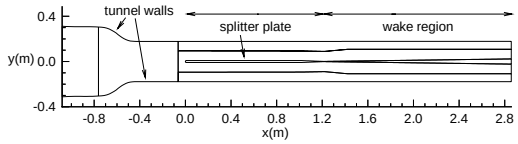

Figure 3. Computational domain for the zero pressure gradient wake test case

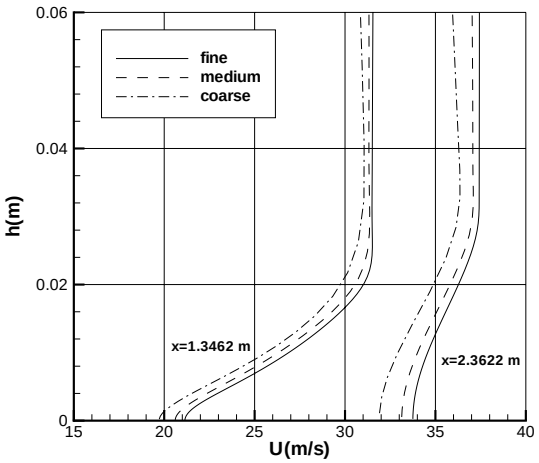

Figure 4. Effect of mesh refinement on the mean velocity for the favorable pressure gradient wake test case - EVM

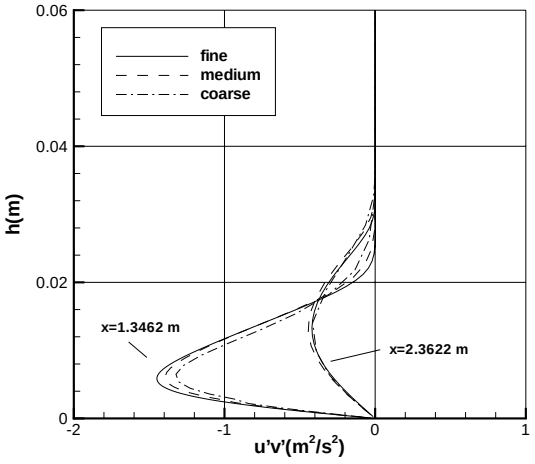

Figure 5. Effect of mesh refinement on the turbulent shear stress for the favorable pressure gradient wake test case - EVM

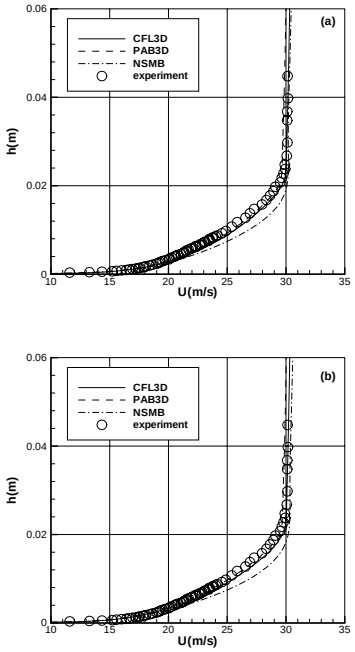

Figure 6. Wake flow with zero pressure gradient - Mean velocity on the splitter plate at $x = 1.2167\ m$: (a)EVM, (b) EASM

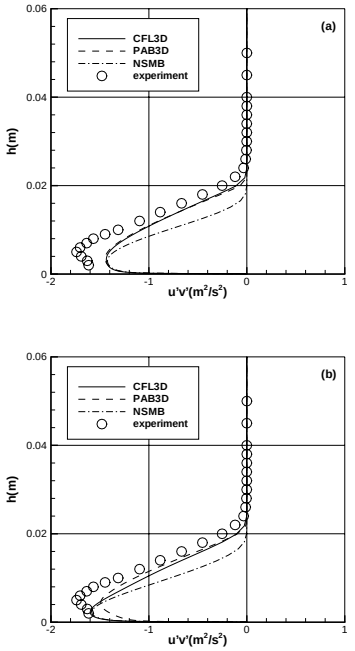

Figure 7. Wake flow with zero pressure gradient - Turbulent shear stress on the splitter plate at $x = 1.2167\ m$: (a)EVM, (b) EASM

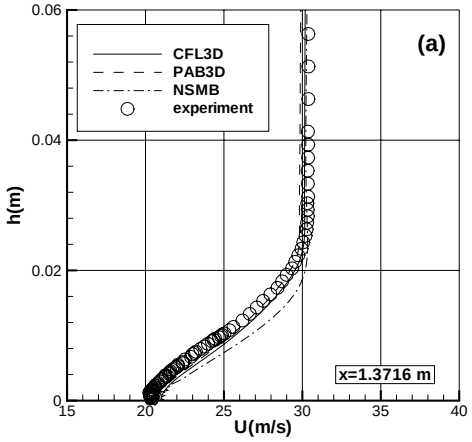

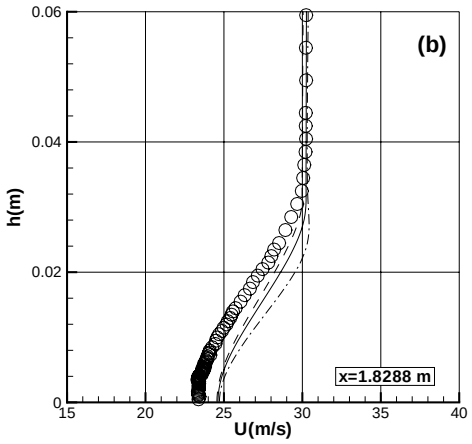

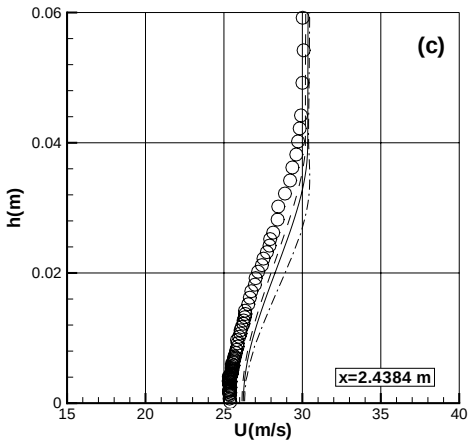

Figure 8. Wake flow with zero pressure gradient - Mean velocity in the wake - EVM

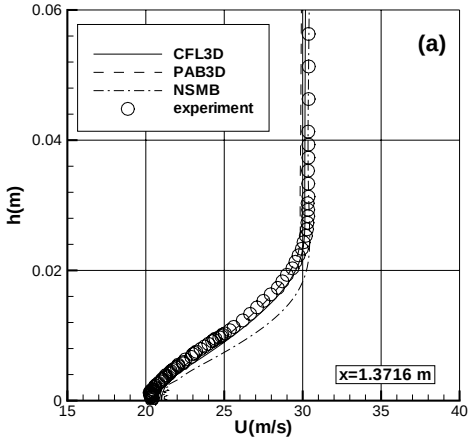

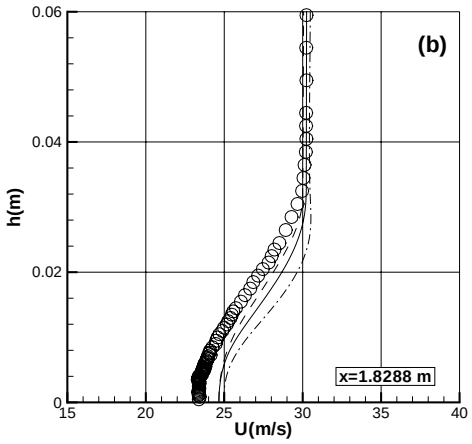

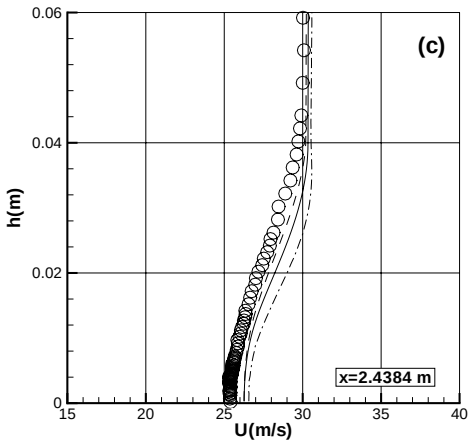

Figure 9. Wake flow with zero pressure gradient - Mean velocity in the wake - EASM

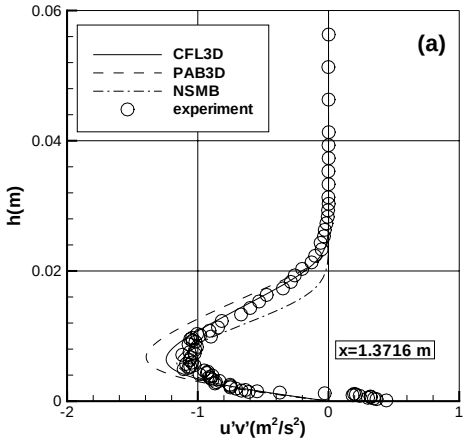

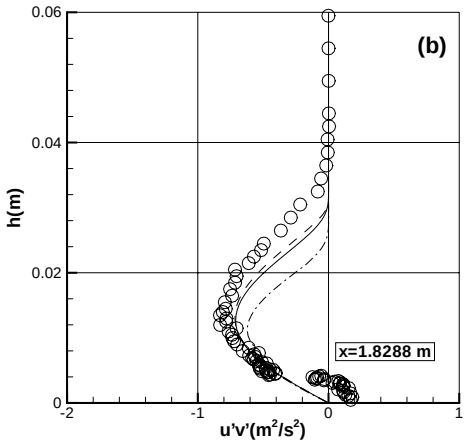

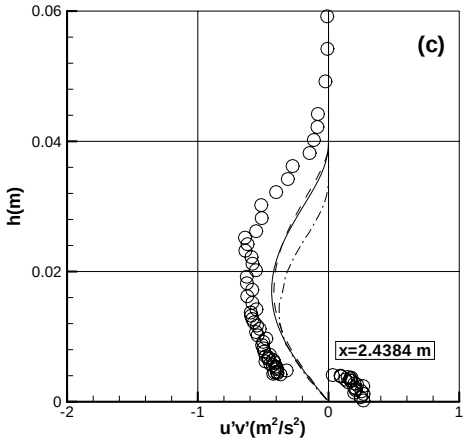

Figure 10. Wake flow with zero pressure gradient - Turbulent shear stress in the wake - EVM

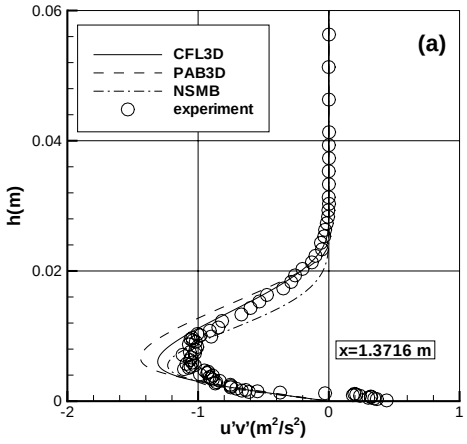

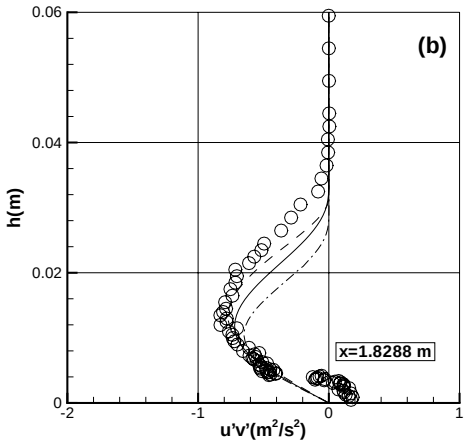

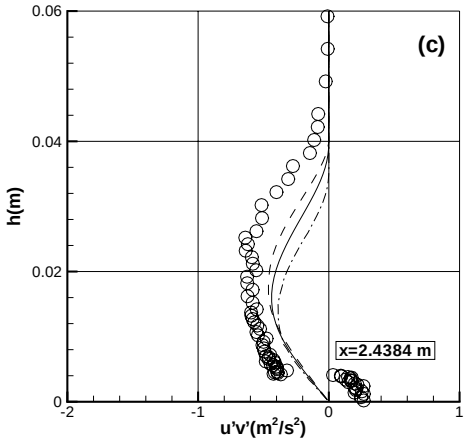

Figure 11. Wake flow with zero pressure gradient - Turbulent shear stress in the wake - EASM

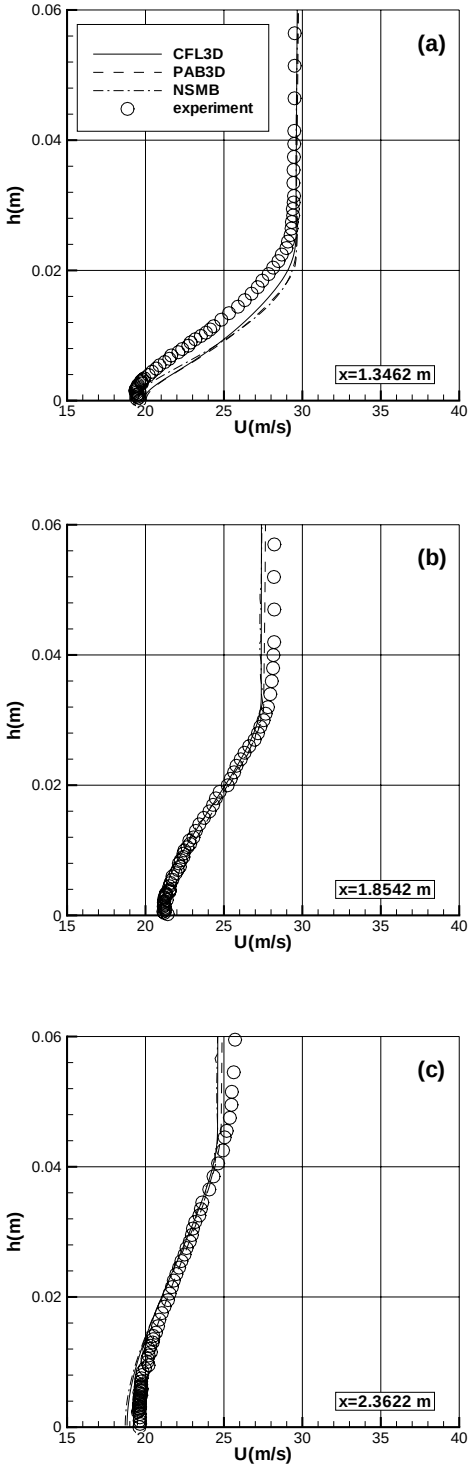

Figure 12. Wake flow with adverse pressure gradient - Mean velocity in the wake - EVM

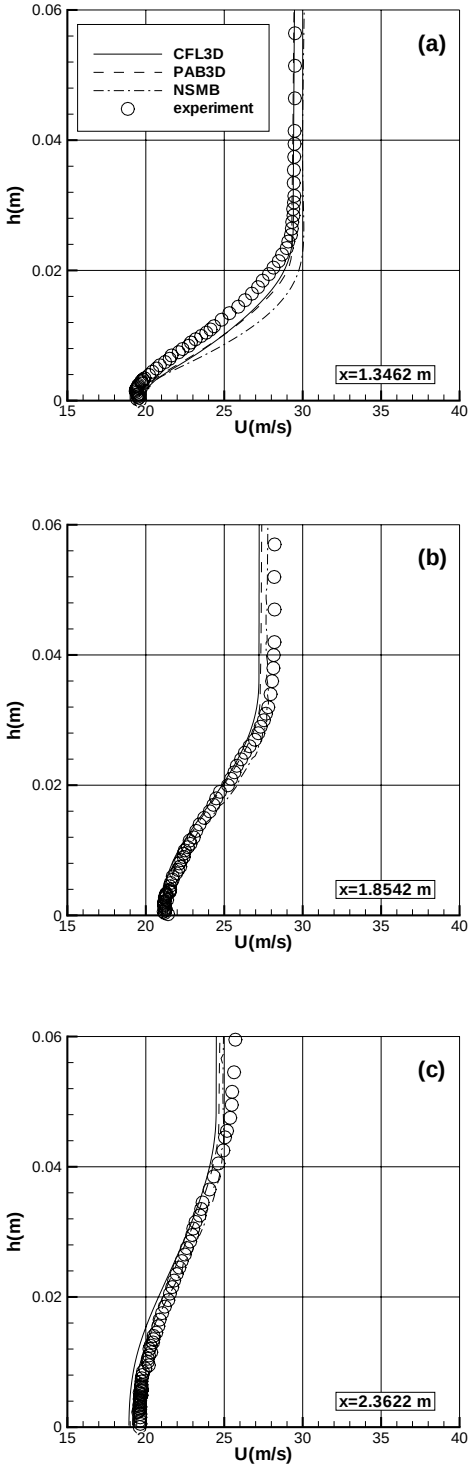

Figure 13. Wake flow with adverse pressure gradient - Mean velocity in the wake - EASM

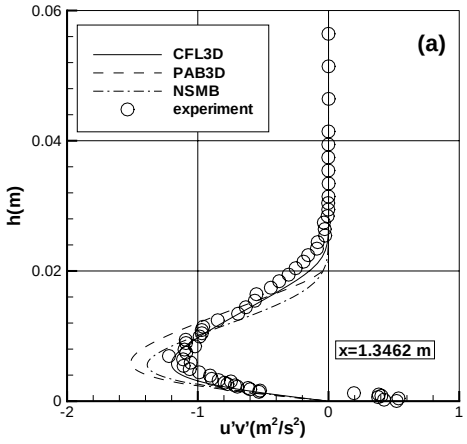

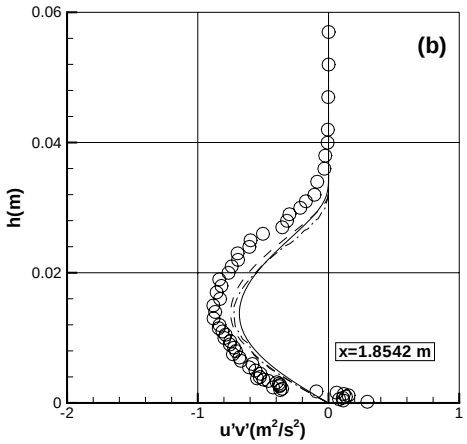

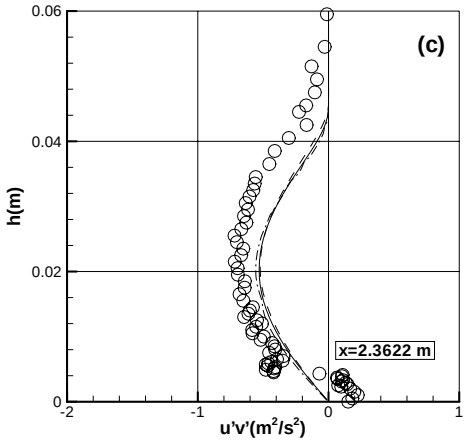

Figure 14. Wake flow with adverse pressure gradient - Turbulent shear stress in the wake - EVM

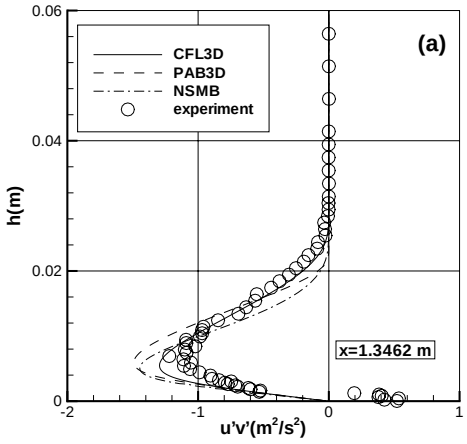

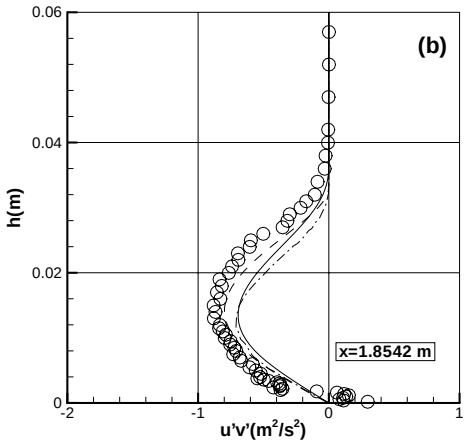

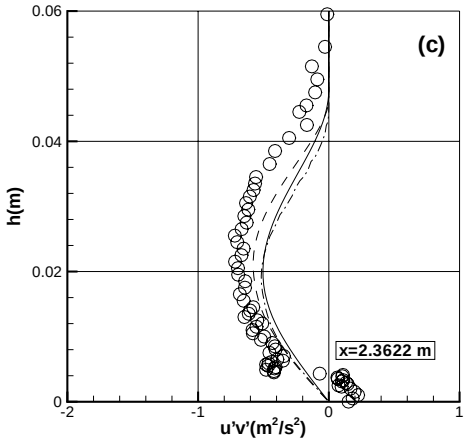

Figure 15. Wake flow with adverse pressure gradient - Turbulent shear stress in the wake - EASM

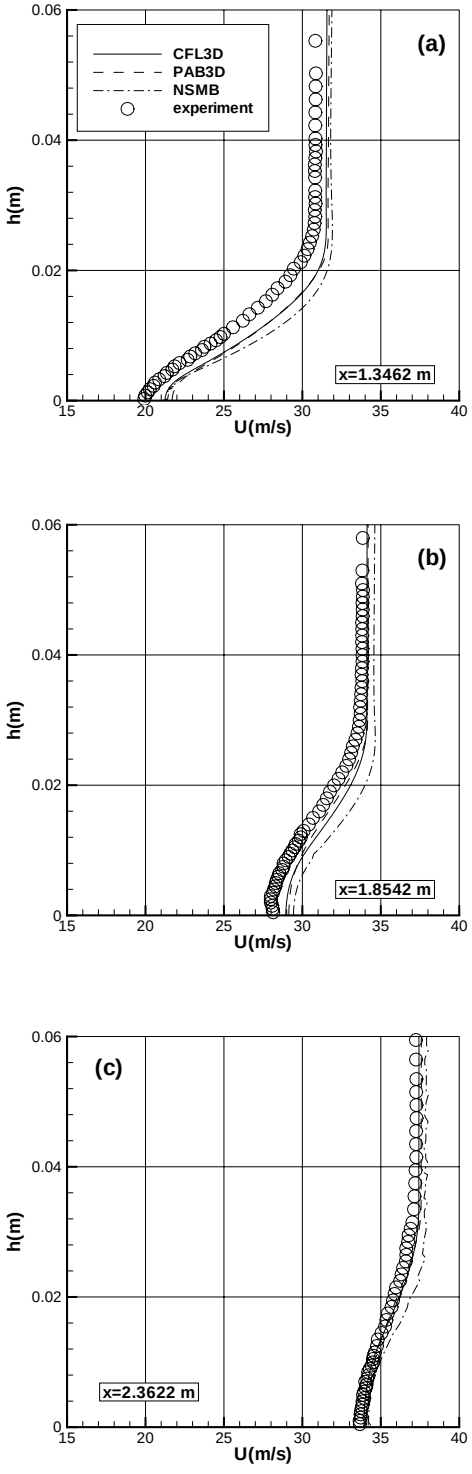

Figure 16. Wake flow with favorable pressure gradient - Mean velocity in the wake - EASM

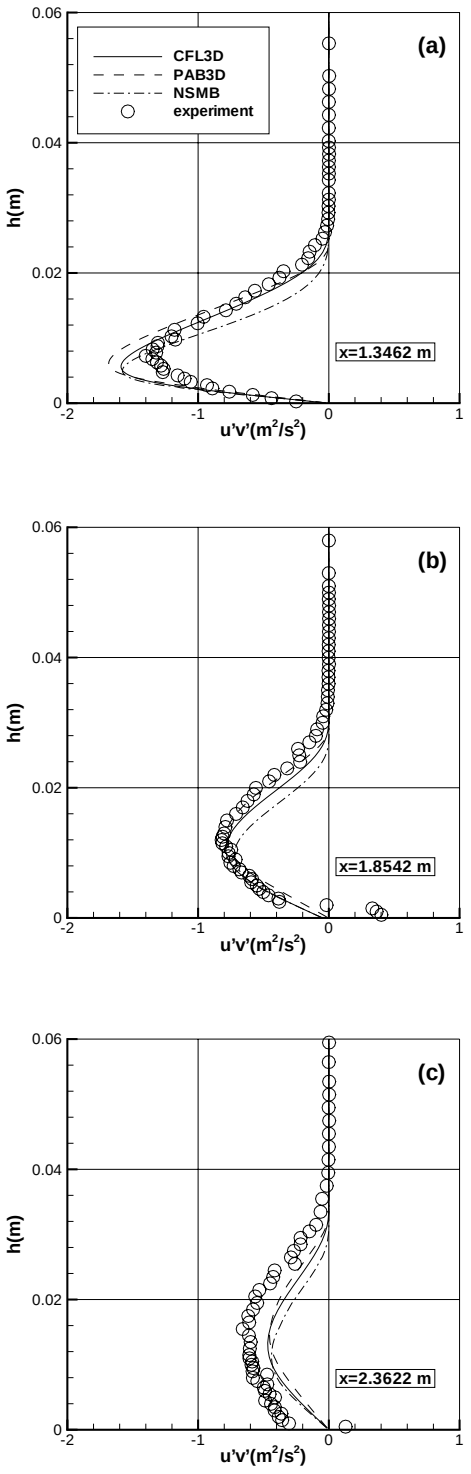

Figure 17. Wake flow with favorable pressure gradient - Turbulent shear stress in the wake - EASM